Angular momentum branching ratios for electron-induced ionization: Atomic and model calculations

M. J. Mehl* and T. L. Einstein
Department of Physics and Astronomy, University of Maryland, College Park, Maryland 20742
(Received 18 March 1987; revised manuscript received 20 May 1987)

We present calculations of the matrix elements for electron-induced ionization of core electrons of atoms. We use both self-consistent atomic potentials for accuracy and model potentials to gain physical insight. We pay particular attention to the angular momentum distribution of the two final-state electrons, especially when one of them lies near what would be the Fermi energy in a solid (i.e., as in an absorption fine-structure experiment). For nodeless core wave functions, in the dominant channel both final-state electrons have angular momentum one greater than that of the initial core state. For sufficiently deeply bound states, this first approximate selection rule holds until the incident electron energy exceeds the ionization threshold by at least 500 eV, i.e., over the experimentally relevant range. It is also possible to determine the angular momentum distribution of the final-state electron. The EXAFS-like electron tends to have angular momentum one greater than that of the initial core state, even in some cases where the first approximate selection rule does not hold. (EXAFS is extended x-ray-absorption fine structure.) The strongest trend is that the dipole component in a partial-wave expansion of the Coulomb interaction dominates the matrix element. In these studies, careful treatment of not just the core state but also the unbound states is crucial; we show that the conventional orthogonalized plane-wave approximation is inadequate, giving incorrect ordering of the channels. For model potentials with an adjustable screening length, low-lying bound resonances are found to play an important role.

I. INTRODUCTION

In this paper we study ionization of an atomic core electron by an incident electron. This problem has received much consideration with regard to the energy dependence of the (inelastic) scattering cross section[1] and the edge singularity.[2] The new question on which we focus is the relative branching ratio (as a function of energy) for various pairs of angular momenta for the two unbound final-state electrons. We are especially interested in the case in which one of these electrons is near threshold (with the other carrying most of the energy). This situation is in contrast to the case of $(e,2e)$ scattering,[3] where the two final-state electrons have similar energy and for which significant simplifications are possible, and to the case of ionization cross sections, where the focus is on the lower-energy electron.[4]

Our motivation stems from our efforts to understand and analyze the extended fine structure found in appearance potential spectroscopy (EAPFS),[5] which we review briefly:[6] In APS an incident electron with energy E_i in the range 500–2000 eV ionizes a core electron with binding energy 250–1500 eV. The excitation probability involves a convolution over the two final-state energies; energy conservation reduces this double integral to a single integral over the energy of a single final-state electron. If the excitation matrix element is slowly varying with energy—an assumption that we verify explicitly—then the only sharp feature in the energy convolution is the unit step function at E_F appearing in the unoccupied density of states. Differentiation (with respect to E_i) produces a δ function at E_F plus a small, smooth derivative of the matrix element. The *derivative* of the oscillatory part of the excitation probability is thus dominated by the case where one final-state electron is at E_F and the other carries the remaining energy E_x.[7,8] Notice that E_x increases linearly with E_i. Hence by monitoring the derivative of the excitation probability as a function of E_i, one has a probe of the excitation probability by counting Auger electrons or soft x rays emitted when the core hole refills or by looking at the decrease in the elastic yield. With E_x a few volts above E_F, APS was originally used to examine the unfilled density of states. For electrons in the range 20–600 eV, the inelastic mean free path is less than 10 Å; then the electron at E_x will not sample the full periodic potential (i.e., the band structure) but rather just the local environment. This argument is just that made in extended x-ray-absorption fine structure (EXAFS) which has been highly successful in determining short-range spacings.[9] Accordingly, we expect to be able to analyze EAPFS using the same relatively simple procedures as in EXAFS. The simplicity of EXAFS analysis depends upon the dipole selection rule, which guarantees that the photoexcited electron has a unique angular momentum. [For a core level with angular momentum $l_c > 0$, calculation confirms the well-known optical result that the channel with angular momentum $l_x = l_c + 1$ dominates the alternative channel with $l_x = l_c - 1$ (Ref. 10)]. With single-channel dominance, one obtains the familiar EXAFS expression in which the near-neighbor spacing R can be extracted from $\sin(2kR + 2\delta_l + \alpha)$, where α is the backscattering

phase from the neighboring atom and δ_l is the (here, well-defined) phase shift due to the excited atom.[11]

Our goal is to show that under certain conditions in EAPFS the electron with energy E_x has predominantly a single angular momentum l_x, and to determine the value of l_x for a given l_c. The key result is that, *when the core wave function is nodeless* (i.e., $1s$, $2p$, $3d$, ...), and *sufficiently deeply bound* (as defined in Sec. IV), an *approximate* dipole rule applies to EAPFS; i.e., $l_x = l_c + 1$. We also confirm that the same l_x dominates over the entire experimental range of E_x (75–500 eV). An additional complication over EXAFS is that there are two "active" electrons rather than just one; hence, we must see how exchange affects the matrix elements. All these problems involve primarily the excitation of the deeply (typically 100 eV or more) bound states of the so-called "central" atom, and so are basically questions of atomic physics. Indeed, Manson has shown that, over most of our range (150–500 eV for Au), photoionization of bulk materials is well described by atomic calculations.[12] The principal contribution of the remainder of the solid is to alter the tails of the wave functions by screening. The more rapid, exponential asymptotic decay of the potential occurs in both our self-consistent local-density potential and our model Yukawa potential. A consequence of using a screened potential is that there will only be a finite number of bound states. It is in this aspect that our studies differ most clearly from those of atomic physicists. We performed some checks (using self-interaction corrected potentials) to show that the use of unscreened core states does not appreciably change the matrix elements.

In another paper[13] we consider this problem more thoroughly by self-consistently embedding an atom in jellium, and present detailed numerical results. In that paper, we also show that using phase shifts appropriate to the correct, pseudodipole selection "rule," as opposed to the originally suspected monopole selection rule,[5,6] does not change stated EAPFS-derived spacings beyond the original error bars when the correct derivative of the data is analyzed. Here we show how most of the relevant physics can be gleaned from a more manageable atomiclike calculation.

In Sec. II we present the general formalism for the problem, including angular momentum combinatorics and simplifications available with angular averaging. In Sec. III we give the results of self-consistent atomic potential computations that support the approximate dipole rule. In Sec. IV, we use model potentials to discuss the physics underlying the numerical trends, especially the improvement of our approximate rules with increasing Z, and show how both the angular momentum factors and the exchange effects enhance dipole relative to the previously believed monopole behavior.[5,6] In Sec. V we summarize the findings of these atomic calculations.

Earlier crude calculations used the orthogonalized plane-wave (OPW) approximation, sometimes employed when the exact continuum electron states are unknown. The hope was that with a good description of the core wave function, one could gain at least a tolerable accounting of the ordering of the matrix elements and other trends of interest. Instead, we show in the Appendix that the OPW underestimates the primary channel by over an order of magnitude, violating the approximate dipole selection rule. In addition, it gives the incorrect energy dependence for the final-state electrons. In short, OPW is notably unreliable.

II. THEORY

The rate of creation of core holes by an incident electron of energy E_i and momentum k_i is given by Fermi's golden rule applied to the spin-averaged transition rate:[14]

$$\langle P_I \rangle = \frac{2\pi N_c}{\hbar} \sum_{\mathbf{k}_1,\mathbf{k}_2:E_1,E_2>E_F} \delta(E_i+E_c-E_1-E_2)\left(\tfrac{3}{4}\,|\,{}_-\langle \mathbf{k}_1\mathbf{k}_2\,|\,V_C\,|\,\mathbf{k}_i\gamma_c\rangle_-\,|^2+\tfrac{1}{4}\,|\,{}_+\langle \mathbf{k}_1\mathbf{k}_2\,|\,V_C\,|\,\mathbf{k}_i\gamma_c\rangle_+\,|^2\right), \quad (1)$$

where $\langle\ \rangle$ indicates an average over the possible magnetic quantum numbers of the core hole, E_c is the core hole binding energy, γ_c represents the quantum numbers of the core electron, and $\mathbf{k}_1,\mathbf{k}_2$ and E_1,E_2 are the wave vectors and energies of the electrons in the final state. The $+$ and $-$ subscripts indicate the symmetry of the wave functions under exchange of the spatial coordinates of the two electrons. The electron-electron Coulomb interaction is denoted by V_C, N_c is the number of scattering sites, and E_F is the Fermi energy (which would be zero in a purely atomic calculation). This *distorted-wave Born approximation* is similar to others widely in use.[4,15–17]

We use the independent-electron approximation, assuming that all the electrons move in a static potential $v(r)$.[18] The problem of many-body effects in EXAFS has received noteworthy attention in recent years.[19] The key result for our work is that EXAFS can be described as a one-electron process, with the overall rate modified by a complicated matrix element due to readjustment of the remaining "passive" electrons. The EXAFS final-state electron wave function should be calculated using a potential which has relaxed around the core hole.[20] (One possibility is the $Z+1$ approximation.[21]) It should furthermore be orthogonal to the initially occupied states of the same angular momentum.[22]

In the usual manner,[23] the calculations reported in this paper involve just the two active electrons and the initial-state potential. Since our primary goal is to evaluate the *relative* strength of various angular momentum combinations rather than their absolute value, we would feel comfortable neglecting many-body relaxation

effects if they essentially introduce only an overall modification of the rate. We performed test calculations to check that such is the case. Since these tests involved atoms embedded in jellium, we will defer detailed discussion to our subsequent paper.[13] In brief, however, we compared calculations using just the initial-state potential to compute both initial- and final-state electrons with others using the final-state potential to compute both final-state wave functions; in both cases, self-interaction corrections[24] were included for the bound state. The matrix element plots of the type of Fig. 1 look very similar, except that the ordinate scale factor is about twice as great in the latter case. It has also been suggested[25] that the ionization rate be calculated in the transition-state model, where both the single-particle orbital to be ionized and the final-state orbital are occupied by one-half electron. Since this means that *both the incident and final states are calculated with the same potential,* one may imagine the model potentials used below to be transition-state potentials. We also considered the scenario that the slower-moving Fermi-level electron screens the potential for the electron at E_x; we accordingly computed the wave functions for the electron at E_F and E_x using the final and initial potentials, respectively, and obtained plots nearly identical to those in which the final potential was used for both electrons.[4,13,26] It is not surprising that the electron at E_x is insensitive to the form of the potential; this result was reported[27] for electrons above about 100 eV, viz., the range of interest. For lower energies, the exchange-correlation potential is quite sensitive to the electron energy.[27,28] Thus our treatment of the Fermi-level electron is far from ideal, but we expect (or hope) that since its energy is fixed, errors in the wave function will primarily introduce errors in the overall magnitude, rather than the relative rates.

We have neglected any final-state correlation effects.[4,29] While such effects can, in general, be important, in the present problem these two electrons have such different energies that interactions between them presumably do not play a major role. Likewise, resonance effects are not expected to be important, except perhaps for the Fermi-level electron.[29]

Under the approximations stated above, the wave functions in (1) are symmetric or antisymmetric combinations of eigenstates of the single-particle Schrödinger equation with potential $v(r)$, having eigenvalues $\mathbf{k}_i$ and γ_c or $\mathbf{k}_1$ and $\mathbf{k}_2$. Our units are chosen so that $\hbar = e^2/2 = 2m = 1$.

The extended fine structure produced by electronic or x-ray probes is, *ipso facto,* a small perturbation on the rate of creation of core holes. Hence, we can start by ignoring all atoms in the system except the one which is to be excited. We will later show that for deeply bound

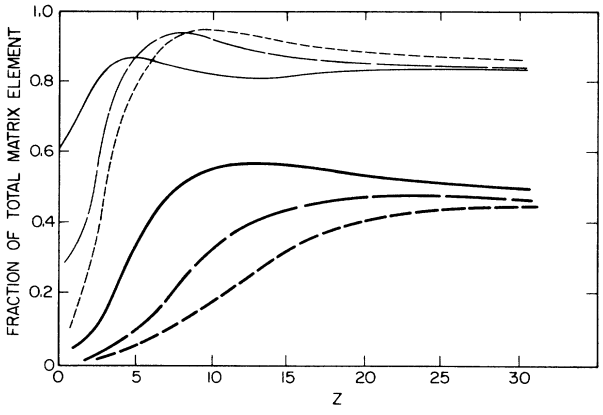

FIG. 1. The upper group of curves shows the fraction of the atomic K-edge ionization rate due to the dipole component ($j=1$) of the Coulomb interaction. The lower group is the fraction of the ionization taking place in the $\{211\}$ channel. Here (——) represents an incident energy 100 eV, (— — —) 500 eV, and (— — —) 1000 eV above threshold 2 $E_F - E_c$. In all cases the second final-state electron is at 13.6 eV.

core states the contributions to the integrals in (1) come exclusively from within the core. The problem thus becomes an essentially atomic one. Hence we approximate the potential v by one which is spherically symmetric about the nucleus of the excited atom, which we take as the origin. Then we can expand the single-particle wave function into partial waves in the usual way,[30] using δ-function normalization for the continuum wave functions.

The transition rate (1) may now be expressed in terms of the radial wave functions. Expanding V_C in spherical harmonics, summing over the magnetic quantum numbers,[31] and changing the integral over momenta into an integral over energy, we find that

$$\langle P_I \rangle \propto \int_{E_F}^{E_x} M(E_i;E_i+E_c-E)\,dE \ , \tag{2}$$

where $E_x = E_i + E_c - E_F$ is the maximum energy of an outgoing electron. The matrix element $M(E_i;E_1,E_2)$ represents the ionization of the core electron by an electron of energy E_i to produce two final-state electrons of energy E_1 and E_2. It may be expressed as a sum over the possible angular momenta of the electrons:

$$M(E_i;E_1,E_2) = \rho(E_1)\rho(E_2) \sum_{l_i,l_1,l_2} M_{l_i l_1 l_2}(E_i;E_1,E_2) \ , \tag{3}$$

where $\rho(E) \propto \sqrt{E}$ is the density of states for electrons at energy E, and

$$M_{l_i l_1 l_2}(k_i^2;k_1^2,k_2^2) = (k_i k_1 k_2)^{-2} \sum_j \Bigg[|F(i,1;2,c;j)|^2 + |F(i,2;1,c;j)|^2 - (-1)^{l_1+l_2} \sum_{j'} \sqrt{(2j+1)(2j'+1)} \begin{Bmatrix} l_i & l_1 & j \\ l_c & l_2 & j' \end{Bmatrix} F(i,1;2,c;j)F(i,2;1,c;j) \Bigg] \ , \tag{4}$$

where the variables j and j' represent the expansion of the Coulomb field into multipole moments, and

$$\begin{Bmatrix} l_i & l_1 & j \\ l_c & l_2 & j' \end{Bmatrix}$$

is the Wigner 6-j symbol.[31] The integral over the radial parts of the wave functions is given by

$$F(i,1;2,c;j)=\left[\frac{(2l_i+1)(2l_1+1)(2l_2+1)}{2j+1}\right]^{1/2} \times \begin{bmatrix} l_i & l_1 & j \\ 0 & 0 & 0 \end{bmatrix} \begin{bmatrix} l_2 & l_c & j \\ 0 & 0 & 0 \end{bmatrix} \times I(i,1;2,c;j) , \quad (5)$$

where

$$\begin{bmatrix} l_i & l_1 & j \\ 0 & 0 & 0 \end{bmatrix}$$

is a Wigner 3-j symbol,[31] and I is the double integral over the radial wave functions:

$$I(i,1;2,c;j)=\int_0^\infty dr_1 \int_0^\infty dr_2 \frac{r_<^j}{r_>^{j+1}} \phi_{k_i l_i}(r_1)\phi_{k_1 l_1}(r_1) \times \phi_{k_2 l_2}(r_2')u_{n_c l_c}(r_2') . \quad (6)$$

The functions $\phi_{kl}(r)/r$ and $u_{n_c l_c}(r)/r$ are solutions of the radial wave equation for the continuum and bound electrons, respectively.

A similar formalism for the distorted Born-exchange approximation has been developed by Rudge and Schwartz[16] and by Younger.[4] Both allow for a phase factor between direct and exchange scattering amplitudes, which is complicated due to the long-range Coulomb interaction. In practice this factor is usually set to unity for convenience.[29] In a solid (our ultimate interest[13]) this long-range interaction is screened, enabling us to neglect this difficulty and so compute the phase "exactly." Younger also projects onto the total angular momentum, which we sum over.

The function $M_{l_i l_1 l_2}(E_i;E_1,E_2)$ defined above is the matrix element for the ionization of a core level (quantum numbers n_c, l_c) by an incident electron of momentum k_i and angular momentum l_i, producing a final state of two continuum electrons, having energies E_1 and E_2 (or momenta k_1 and k_2) and angular momenta l_1 and l_2, respectively. Note that E_1 and E_2 may take on any energies above the Fermi level allowed by the conservation law, $E_i+E_c=E_1+E_2$. In addition, although the total angular momentum of the system is of course conserved, there are many possible combinations of (l_1,l_2) for a given (l_i,l_c), in contrast to EXAFS.[10,32,33]

III. SELF-CONSISTENT POTENTIAL CALCULATIONS

In the preceding section we developed a formula for the transition rate as a sum over the possible angular momentum channels $\{l_i l_1 l_2\}$ of the incident and final-state electrons. If one such channel dominates the transition rate (2), then the analysis will immediately simplify to one much like that used in EXAFS, allowing relatively easy discovery of the environment of an atom near the surface of a bulk material. In this section and the next we present evidence for the presence of an "approximate selection rule" which indicates the particular channel which dominates the ionization rate. We also determine the range of experimental conditions over which such behavior holds. The weakest aspect of this calculation is the treatment of the Fermi-level electron. In addition to its sensitivity to details of the potential, the associated nontrivial angular momentum dependence of the density of states in a material (i.e., the part not proportional to $2l+1$) may modify our results.

Our first calculations used potentials derived from the atom-in-jellium model of Bryant.[20] This local-density-approximation model should accurately portray the behavior of the electrons near a nucleus in a metal. However, evaluation of these potentials takes large amounts of computer time and the physics behind the results is difficult to understand. As discussed in the Introduction, we restrict ourselves to atomiclike calculations with screening by the background reflected only in the exponential decay of the potential.

We generate atomic potentials using the local-density approximation of density-functional theory.[3,4] Specifically, we use a modification of the code developed by Herman and Skillman,[35] which produces a nonrelativistic self-consistent electron density and single-particle potential. Calculations were performed both with and without orbital-dependent self-interaction corrections.[20,24] While one must note that neither the incident electron nor the scattered final-state electrons move in this potential (which is accurate only for the bound electrons),[36] inclusion of more accurate, energy-dependent potentials[27,28] does not change our basic results. We will discuss these corrections in our next paper.

We begin by generating self-consistent spherically averaged charge densities and potentials for all atoms with atomic number $Z<33$. We used only l's ≤ 6. These potentials are used to create the wave functions to be used in evaluation of the matrix element (4). Since the important quantity in EAPFS, as in EXAFS, is the energy above threshold, we considered incident electron energies 100, 500, 1000 eV above the ionization threshold, $|E_c|+2E_F$. To approximate the environment in which EAPFS is to be measured, we set $E_F=1$ Ry, or 13.6 eV. Since we are primarily interested in EAPFS-like properties, we fix one of the final-state electrons at the Fermi level, $E_2=E_F$.

For the ionization of 1s and 2p electrons (K- and $L_{2,3}$-edge processes), we find the key result that at low energies above threshold, one channel dominates the ionization rate. In K-edge excitations it is the $\{211\}$ chan-

nel, while for the $L_{2,3}$ edge it is $\{322\}$. The results are summarized by the thick lines in Figs. 1 and 2. These lines represent the fraction of the total ionization rate which goes into the preferred channel at each energy. The K-edge process is clearly dominated by the $\{211\}$ channel, with up to 45% of the ionization going into this channel for $Z > 10$ when the incident energy is less than 500 eV above threshold. The $L_{2,3}$ edge is not so clearly dominated by the $\{322\}$ channel, but for $Z > 15$ at least 30% of the ionization goes into this channel for incident energies on the order of 100 eV above threshold, although there is a rapid fall-off with increasing energy. As Z increases, the fractional contribution of the $\{322\}$ channel also increases.

The presence of these preferred channels means that a large fraction of the higher final-energy, EXAFS-like electrons will have an EXAFS-like angular momentum, i.e., $l_x = l_c + 1$. Although in EAPFS the selection "rule" is not nearly so well satisfied as it is in EXAFS, the fraction of EAPFS electrons with EXAFS-like angular momentum is large enough so that EAPFS can be used to determine atom separations in solids.[13]

Referring to Eqs. (3)–(6), we see that both of these preferred channels are produced by the dipole ($j = 1$) part of the Coulomb interaction between the incident and core electrons. The contribution to the ionization (3) from the $j = 1$ part of the Coulomb potential for both edges is shown as the thinner (and upper) lines in Figs. 1 and 2. The dipole part of the potential quite clearly dominates the ionization, and at least in the K-edge case seems to be increasing in relative strength with increasing energy. This may not seem particularly surprising, since the dipole part of the interaction is known to dominate in the case of small momentum transfer.[37] In this case, however, there is no *a priori* reason to expect small momentum transfer. For example, in the case of aluminum, orthogonalized plane-wave (OPW) calculations suggested that the monopole part of the potential dominated the interaction[38] (cf. Appendix).

Since the aluminum and oxygen K-edge excitations have been investigated experimentally,[6,37] we pay particular attention to them here. In Table I we list the fraction of the ionization (3) coming from the dipole part of the Coulomb interaction, the fraction of EXAFS-like electrons with the EXAFS-like angular momentum ($l_x = 1$), and the fraction of ionization events which take place in the $\{211\}$ channel, as a function of energy above threshold when $E_2 = E_F$. We include both self-interaction corrected[24,39] (SIC) and strict local-density-approximation (LDA) atomic potentials. In the former the *core* wave functions are Coulomb-like at large distance, while in the latter, the core wave functions are those appropriate to a screened potential and thus more closely approximate the core states in a metal.[40] Looking at Table I, we see that the difference between SIC and LDA calculations is quite small, indicating that the behavior of the tail of the core-state wave function has little effect on the matrix element.

Table I shows that the contribution of the $\{211\}$ channel falls off rapidly with increasing E_i in oxygen, but not so rapidly in aluminum. This is in keeping with the trends shown in Fig. 1, where we see that at larger Z the fraction of electrons in the preferred channel is almost independent of energy. Of course, the $\{211\}$ channel is not the only one which contributes $l_x = 1$ electrons. When we add the other channels, we find that over half of the aluminum ionizations produce $l_x = 1$ electrons if the E_i is no more than 500 eV above threshold. At 200 eV above the oxygen edge only 30% of the events are in the $\{211\}$ channel, but about 50% of them contribute $l_x = 1$ electrons. The $l_x = 1$ channels dominate until about 500 eV above threshold, when the $l_x = 2$ channels take over. In both aluminum and oxygen, however, the dipole part of the Coulomb interaction is by far the major driver of the ionization.

To examine the behavior of an $L_{2,3}$-edge excitation, we did calculations for the ionization of a titanium $2p$ electron. The results are also listed in Table I. The preferred $\{322\}$ channel is the largest channel for energies 400 eV or less above threshold, the most likely angular momentum of the EXAFS-like electron is $l_x = 2$ for energies within 800 eV of threshold, and the interaction is dipole dominated for all energies. As seen in Fig. 2, these trends will improve as we go to larger values of Z.

We went beyond $Z = 33$ to examine the possibility of EXAFS-like behavior of an $M_{4,5}$ excitation. As will be shown below, such an excitation should have a preferred $\{433\}$ channel, with $l_x = 3$ as the dominant angular momentum of the highest-energy final-state electron. We found no evidence of this trend for copper, rhodium, or silver, which were in fact monopole dominated, but we found a very strong dipole and single channel dominance in barium ($Z = 56$) as is shown at the bottom of Table I. In barium the $\{433\}$ channel is the largest one for energies up to 800 eV above threshold, and the EXAFS-like electron has at least a 40% chance of being in the $l_x = 3$ state for energies within 1000 eV of threshold. The fact that barium follows our expectations so well indicates that the trend is followed for some atoms with smaller atomic numbers than barium, although we have not calculated the atomic number at which this behavior starts.

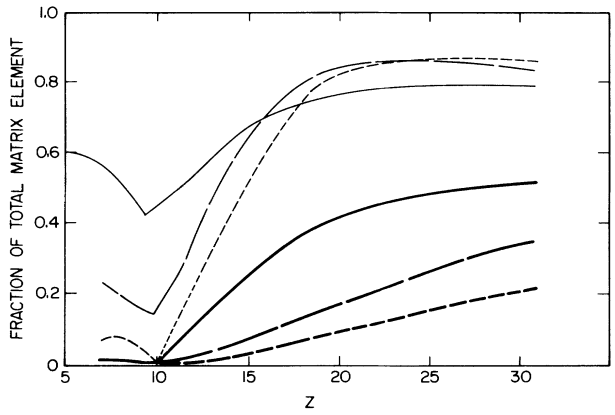

FIG. 2. The $L_{2,3}$-edge ionization. The notation is the same as in Fig. 1, except that the lower set of curves represents the $\{322\}$ ionization fraction.

TABLE I. Percentage of the ionization rate (3) with the listed property when $E_2 = E_F$.

Oxygen—self-consistent field with self-interaction correction

Energy above K threshold (eV)	$j=1$	$l_x=0$	$l_x=1$	$l_x=2$	{211}
100	79.2	19.6	62.1	15.9	40.9
200	85.0	14.6	51.0	25.3	31.7
300	88.5	11.3	42.4	29.5	25.0
400	90.4	9.1	36.2	30.9	20.3
500	91.5	7.7	31.7	31.2	17.0
600	91.9	6.7	28.4	30.9	14.6
800	91.7	5.5	24.0	29.7	11.5
1000	90.8	4.8	21.3	28.5	9.6

Oxygen—self-consistent field without self-interaction correction

Energy above K threshold (eV)	$j=1$	$l_x=0$	$l_x=1$	$l_x=2$	{211}
100	81.7	17.1	61.6	18.1	41.5
200	87.8	12.5	49.2	27.2	31.3
300	91.3	9.6	40.3	30.7	24.3
400	93.3	7.7	34.1	31.5	19.5
500	94.3	6.5	29.7	31.3	16.3
600	94.7	5.7	26.6	30.7	14.0
800	94.6	4.7	22.5	29.3	11.0
1000	93.8	4.1	20.0	28.0	9.2

Aluminum—self-consistent field with self-interaction correction

Energy above K threshold (eV)	$j=1$	$l_x=0$	$l_x=1$	$l_x=2$	{211}
100	75.9	22.6	69.1	8.0	46.6
200	78.6	20.3	64.3	13.9	42.4
300	81.1	18.2	59.7	18.8	38.6
400	83.2	16.4	55.5	22.5	35.2
500	84.9	14.8	51.6	25.4	32.1
600	86.4	13.5	48.1	27.4	29.3
800	88.7	11.3	42.2	30.0	24.8
1000	90.2	9.7	37.6	31.1	21.3

Aluminum—self-consistent field without self-interaction correction

Energy above K threshold (eV)	$j=1$	$l_x=0$	$l_x=1$	$l_x=2$	{211}
100	77.2	21.0	69.7	8.9	47.6
200	80.1	18.8	64.3	15.2	43.1
300	82.6	16.8	59.3	20.2	38.9
400	84.8	15.1	54.7	23.9	35.2
500	86.7	13.6	50.6	26.6	32.0
600	88.2	12.3	47.0	28.5	29.1
800	90.5	10.3	41.0	30.7	24.4
1000	92.0	8.8	32.3	31.6	20.9

TABLE I. (*Continued*).

Titanium—self-consistent field with self-interaction correction

Energy above $L_{2,3}$ threshold (eV)	$j=1$	$l_x=1$	$l_x=2$	$l_x=3$	$\{322\}$
100	62.9	30.2	57.1	9.2	37.7
200	67.1	24.9	50.0	18.4	31.3
300	69.9	21.2	44.2	23.8	26.3
400	71.5	18.6	39.9	26.8	22.5
500	72.3	16.8	36.7	28.5	19.6
600	72.4	15.6	34.3	29.5	17.5
800	71.6	14.0	31.0	30.2	14.5
1000	70.0	13.1	28.9	30.3	12.5

Titanium—self-consistent field without self-interaction correction

Energy above $L_{2,3}$ threshold (eV)	$j=1$	$l_x=1$	$l_x=2$	$l_x=3$	$\{322\}$
100	65.4	28.2	57.6	10.4	39.0
200	69.7	23.2	49.6	19.9	31.7
300	72.5	19.7	43.4	25.1	26.2
400	74.1	17.4	39.0	27.8	22.2
500	74.8	15.8	35.8	29.3	19.4
600	74.9	14.7	33.4	30.0	17.2
800	74.0	13.3	30.2	30.5	14.2
1000	72.4	12.6	28.3	30.5	12.3

Barium—self-consistent field without self-interaction correction

Energy above $M_{4,5}$ threshold (eV)	$j=1$	$l_x=2$	$l_x=3$	$l_x=4$	$\{433\}$
100	75.3	26.8	65.6	2.1	50.9
200	76.0	24.8	61.3	8.0	46.3
300	76.9	22.7	57.0	14.3	41.9
400	77.5	20.9	53.2	19.7	38.1
500	77.8	19.6	50.1	24.0	35.0
600	77.9	18.5	47.6	27.3	32.4
800	77.6	17.1	43.8	32.0	28.5
1000	76.7	16.2	41.1	34.9	25.6

Barium—self-consistent field without self-interaction correction

Energy above $M_{4,5}$ threshold (eV)	$j=1$	$l_x=2$	$l_x=3$	$l_x=4$	$\{433\}$
100	76.3	25.5	66.7	2.3	52.3
200	77.0	23.6	62.0	8.7	47.2
300	77.8	21.5	57.2	15.3	42.3
400	78.4	19.9	53.2	20.8	38.3
500	78.7	18.6	49.9	25.1	35.0
600	78.8	17.7	47.3	28.4	32.3
800	78.4	16.4	43.5	33.0	28.3
1000	77.5	15.6	40.8	35.8	25.4

IV. MODEL CALCULATIONS

In the preceding section we found that the ionization is driven almost entirely by the dipole part of the Coulomb interaction between the incident and core electrons, and that, at least for the K-, $L_{2,3}$-, and $M_{4,5}$-edge excitations, and for sufficiently large atomic numbers, a preferred channel for the incident and outgoing angular momenta exists. We will refer to these findings as the "approximate dipole" and "approximate EXAFS" selection rules, respectively.

These "rules" may be the result of the distorted-wave Born approximation, although this seems improbable based on Geltman's[15] previously cited calculations, or of the choice of single-particle potential, which is strictly valid only for determining the ground-state charge density. To alleviate the latter concern and show that our results are insensitive to the details of the potential, we here study a set of model potentials with variable parameters. We will show under what conditions our two "approximate" selection rules hold.

To represent an ion screened by the conduction electrons in a metal, we use a simple Yukawa-like potential:

$$v(r)=-\frac{2Z}{r}e^{-r/a}, \tag{7}$$

where a is a screening length. Changing Z and a generates a large class of potentials, qualitatively similar to single-particle potentials found in Sec. III and in more realistic models.[39] We also used a potential generated by a point charge surrounded by a neutralizing, spherical shell. This potential produced results similar to those reported below.

For K-edge excitations, Sec. III indicates that the dominant channel in the system will be the one we have labeled $\{211\}$. To stay with an aluminumlike system we set $Z=13$. To gauge a, we note that $a=0.4$ a.u. produces a $1s$ eigenstate bound by 1530 eV, close to the ESCA (electron spectroscopy for chemical analysis) binding energy of 1560 eV.[41] For specificity, we again set the Fermi level at 1 Ry and consider only an incident electron with energy 100 eV above the threshold: $E_i=2E_F-E_c+100$ eV. (Remember that the threshold process leaves both electrons at the Fermi level.) Note that E_i is not constant, since the core-level binding energy E_c will change as we change the screening parameter a. In Fig. 3, we treat two special cases for the final-state electron energies. In this figure we see that neither the approximate EXAFS rule nor the weaker approximate dipole rule dominates until $a>0.2$. There the $\{211\}$ channel rises suddenly to approximately 70% of the ionization rate and the dipole term contributes 90% of the total ionization rate at about $a=0.3$. The ratio of $\{211\}$ to the total ionization then decays as a increases, but the $\{211\}$ channel still accounts for 40% of the final-state matrix element at $a=1.0$. Note that the dipole contribution remains relatively constant for all $a>0.3$, including the "physical" value $a=0.4$.

In Fig. 4 we show similar results for the $L_{2,3}$ edge of the $Z=22$ potential, chosen to understand the experimental Ti data.[42] The predicted dominant channel,

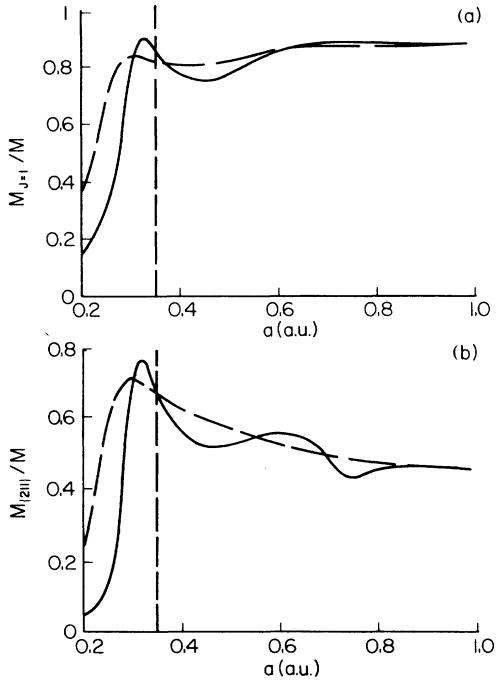

FIG. 3. Fraction of the total matrix element going into a single channel. Shown is the K-edge excitation of the Yukawa potential (7) with $Z=13$, as a function of the screening length a. The incident electron's energy is 100 eV above the ionization threshold. (——) represents the case $E_2=E_F=13.6$ eV. (— —) represents the case $E_1=E_2=E_F+50$ eV. (a) The ratio of the dipole matrix element [those parts of (3) with both $j=j'=1$] to the total matrix element (3). (b) The ratio of the $\{211\}$ channel matrix element (4) [including the density of states proportional to (k_1k_2)] to the total matrix element. The vertical dashed line represents the point at which the $2p$ resonance energy is at the Fermi level.

$\{322\}$, does indeed dominate once $a>0.45$, although the dominance is not as sizable as in the K-edge process. In this case the "physical" value of a is 0.375, where the $2p$ binding energy is about 460 eV. This is just barely in the region of $\{322\}$ dominance when one of the electrons is near the Fermi level. As seen in Table I, in a more realistic Ti potential the ionization is indeed dominated by the $\{322\}$ channel, as we shall corroborate in detail in a future paper.[13]

To test an $M_{4,5}$ edge, we choose $Z=29$ to replicate Cu, and study the ionization of a $3d$ core level in Fig. 5. (The $M_{4,5}$ edge of Cu is about 2 eV,[41] so the "physical" value of a is about 0.5.) The approximate EXAFS selection rule defined above would predict that the dominant channel would be $\{433\}$. Note that the $j=1$ channel is again largest for $a>0.6$, although when one electron is at the Fermi level there is a large oscillation in the dipole contribution. The approximate EXAFS selection rule is not followed very strongly, since it can drop to as low as 20% when one electron is at the Fermi level. As we mentioned in the preceding section, a self-consistent Cu potential shows monopole, not dipole dominance, while the Ba potential satisfies both of the approximate rules.

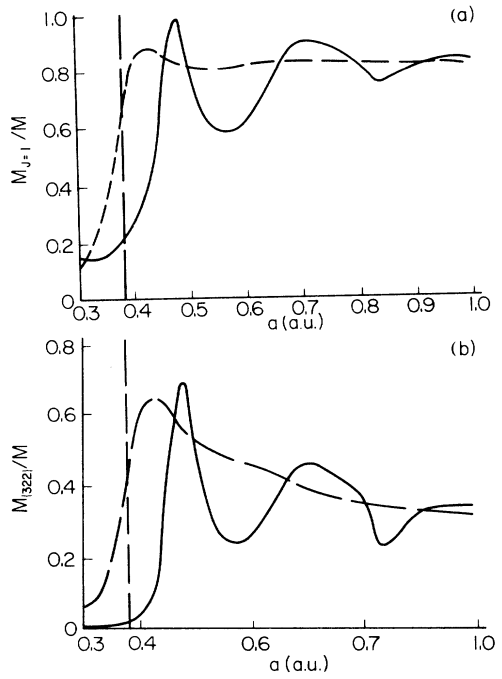

FIG. 4. Fraction of the total matrix element going into a single channel. The conditions are the same as in Fig. 3 except that we look at the ionization of a $2p$ electron in the $Z=22$ Yukawa potential, and (b) is the ratio of the $\{322\}$ channel to the total matrix element. The vertical dashed line represents the point at which the $3d$ resonance energy is at the Fermi level.

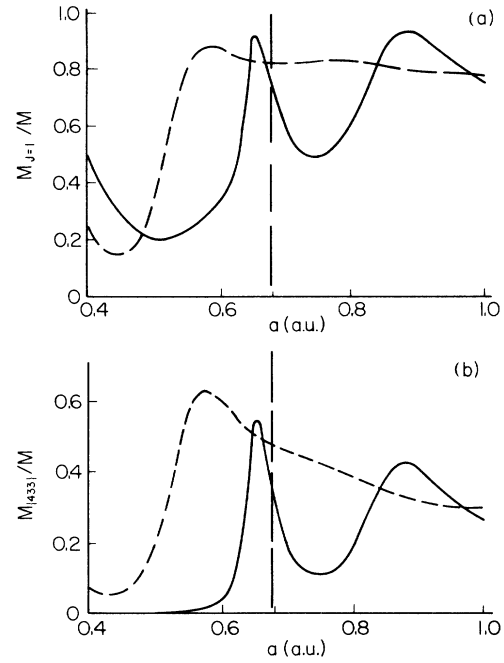

FIG. 5. Fraction of the total matrix element going into a single channel. The conditions are the same as in Fig. 3 except that we look at the ionization of a $3d$ electron in the $Z=29$ Yukawa potential, and (b) is the ratio of the $\{433\}$ channel to the total matrix element. The vertical dashed line represents the point at which the $4f$ resonance is at the Fermi level.

What mechanism generates the approximate dipole and approximate EXAFS selection rules? We believe it is the onset of the $2p$ bound state for the K edge, the $3d$ bound state in the $L_{2,3}$ excitation, and the $4f$ bound state when ionizing the $M_{4,5}$ edge. By examining the bound-state eigenvalues and resonances of the Yukawa potential as a function of Z and a, we find that the $Z=13$ $2p$ state becomes resonant at about 60 eV when $a=0.28$, the $Z=22$ $3d$ state is resonant at about 10 eV when $a=0.4$, and the $Z=29$ $4f$ state is resonant at about 35 eV when $a=0.6$. At slightly larger values of a these states become bound. These resonance-producing values of a mark the approximate lower limit of validity of our approximate selection rules. Our physical interpretation (for the K edge) is that below the resonance ($a<0.28$ when $Z=13$), the $l=1$ wave function at energies E between E_F and E_x is very small in the core region. The $l=0$ wave function is rather large there, since (at all energies) it must be orthogonal to the $1s$ bound state. Thus the final-state electrons tend to have angular momentum 0, and we have an approximate monopole selection rule. When a is sufficiently large for a $2p$ resonance (or bound state) to exist, the $l=1$ final states above the resonance energy must be orthogonal to a wave function which is large in the core region, and so must also be large there. Consequently at values of a above the resonance the $l=1$ final state is favored. These arguments apply in an analogous manner to changes in the nuclear charge Z.

We summarize some of the numerical calculations supporting the above claims in a series of tables. In Table II we compare the radial integral I in Eq. (6) for the $\{000\}$ and $\{211\}$ channels when a K-shell electron is ionized. We use the Yukawa-like potential (7) with $Z=13$, and assume an incident energy 100 eV above the threshold. The column labeled "EXAFS" gives the process in which the core electron goes to E_x, as in EXAFS, with the incident electron dropping to E_F. In the "exchange" process, the reverse occurs. Note that the ratio of the $\{211\}$ to $\{000\}$ excitation rates rises rapidly around $a=0.3$ as we go through the $2p$ resonance. The radial integral (6) is related to the single-channel matrix element by the rather complicated expression (4). To clarify the relationship, we present in Table III several radial integrals and the associated matrix elements. In this case the $\{211\}$ radial integrals are approximately three times as large as the $\{000\}$ radial integrals. If there were no angular momentum factors in (4), the ratio of the $\{211\}$ to $\{000\}$ matrix elements would thus be about nine to one. Instead, the actual ratio is about 6.5 to 1. The effects of other channels can be seen by comparing ratios of other radial integrals to the appropriate matrix elements.

Since the $\{211\}$ channel is activated when the $2p$ resonance appears, we should check what happens when the potential becomes deep enough to support a $3d$ resonance; e.g., a quadrupole channel, say $\{422\}$, might dominate. In Table IV we dispose of this concern. The table shows the radial integrals (6) and matrix elements (4) for different channels, for the $Z=13$ potential of Table II and $E_i-2E_F+E_c=100$ eV. The $\{211\}$ state

TABLE II. Comparison of {000} and {211} radial integrals [Eq. (6)]. $E_i = 2E_F - E_{1s} + 100$ eV ($E_F = 13.6$ eV); K-shell excitation.

	$E_1 = 100$ eV $+ E_F$, $E_2 = E_F$			
	{000} channel		{211} channel	
a (a.u.)	EXAFS	Exchange	EXAFS	Exchange
0.2	2.74×10^{-4}	2.56×10^{-4}	1.21×10^{-4}	1.14×10^{-4}
0.3	2.32×10^{-4}	2.20×10^{-4}	9.50×10^{-4}	9.09×10^{-4}
0.4	1.57×10^{-4}	1.50×10^{-4}	4.90×10^{-4}	4.72×10^{-4}
0.5	1.68×10^{-4}	1.61×10^{-4}	4.87×10^{-4}	4.69×10^{-4}

	$E_1 = E_2 = 50$ eV $+ E_F$	
a (a.u.)	{000} channel	{211} channel
0.2	2.20×10^{-4}	2.23×10^{-4}
0.3	1.79×10^{-4}	9.42×10^{-4}
0.4	1.36×10^{-4}	5.04×10^{-4}
0.5	1.26×10^{-4}	4.46×10^{-4}

TABLE III. Comparison of radial integrals [Eq. (6)] and matrix elements [Eq. (4)]. Yukawa potential $Z = 13$, $a = 0.4$; $E_2 = E_F$.

Channel	EXAFS	Exchange	Total matrix element
{000}	1.50×10^{-4}	1.57×10^{-4}	6.84×10^{-8}
{211}	4.68×10^{-4}	4.87×10^{-4}	4.40×10^{-7}
{321}	7.34×10^{-5}	1.14×10^{-4}	2.89×10^{-8}
{312}	1.00×10^{-5}	6.62×10^{-6}	2.22×10^{-9}
{431}	5.05×10^{-6}	1.48×10^{-5}	7.34×10^{-10}
{413}	4.21×10^{-7}	1.32×10^{-7}	6.04×10^{-13}

TABLE IV. Radial integrals and matrix elements. Yukawa potential $Z = 13$; $E_1 = E_2 = 63.6$ eV.

Radial integrals [Eq. (6)]

	Channel				
a (a.u.)	{000}	{211}	{321}	{312}	{422}
0.1	58.6×10^{-5}	53.9×10^{-5}	23.2×10^{-5}	17.3×10^{-5}	9.07×10^{-5}
0.2	22.0	22.3	2.72	1.80	0.32
0.3	17.9	94.2	5.58	3.62	0.34
0.4	13.6	50.4	6.35	4.13	0.86
0.5	12.6	44.6	10.5	6.86	2.70
0.6	12.0	42.6	14.9	9.80	5.78
0.7	11.4	40.0	16.3	10.8	7.42
0.8	11.0	38.1	16.5	11.0	8.09
0.9	10.7	36.7	16.6	11.1	8.56
1.0	10.5	35.7	23.6	15.6	8.93

Total matrix elements [Eq. (4)]

	Channel			
a (a.u.)	{000}	{211}	{321} = {312}	{422}
0.1	161×10^{-8}	90.4×10^{-8}	18.9×10^{-8}	1.98×10^{-8}
0.2	22.6	15.5	0.26	0.002
0.3	14.9	276	1.11	0.003
0.4	8.60	79.2	1.44	0.018
0.5	7.42	62.1	3.90	0.176
0.6	6.70	56.5	7.86	0.804
0.7	6.09	50.0	9.42	1.32
0.8	5.66	45.2	9.69	1.57
0.9	5.36	42.0	9.84	1.76
1.0	5.14	39.7	12.2	1.92

TABLE V. L_1-edge matrix elements [Eq. (4)]. Yukawa potential $Z=13$; $E_1=E_2=63.6$ eV.

	Channel			
a (a.u.)	{000}	{211}	{422}	{413}
0.4	12.9×10^{-6}	0.0694×10^{-6}	68.6×10^{-6}	5.28×10^{-6}
0.5	6.27	0.562	70.0	2.77
0.6	3.76	0.966	70.2	0.563
0.7	2.55	0.975	41.6	2.07
0.8	1.91	0.897	24.2	2.33
0.9	1.52	0.820	16.0	2.62
1.0	1.28	0.756	11.7	2.80

dominates for $a>0.3$ (the $2p$ onset), even after the potential supports a $3d$ resonant or bound state at about $a=0.6$. Although we tabulate only the case $E_2=E_1$, the slowly changing nature of the matrix element causes the behavior of the {211} channel to remain dominant even when $E_2=E_F$, as a careful examination of Fig. 3 will show.

When the core state has nodes, the results are strikingly different. In Fig. 6 and Table V we show the matrix elements for an L_1 excitation, using the same Yukawa potential. The approximate EXAFS selection rule clearly fails drastically in this case. The approximate dipole selection rule also fails, since the largest matrix element for L_1 excitation is {422}, produced entirely by the quadrupole part of the Coulomb interaction. There are claims of dipole excitation above the M_3 edge for reflection surface extended energy loss fine structure for various materials.[43,44] A justification given for the claim is that elastic backscattering is followed by small-angle inelastic scattering.[43,44] We are investigating this situation by including the appropriate angular factors into our theory.

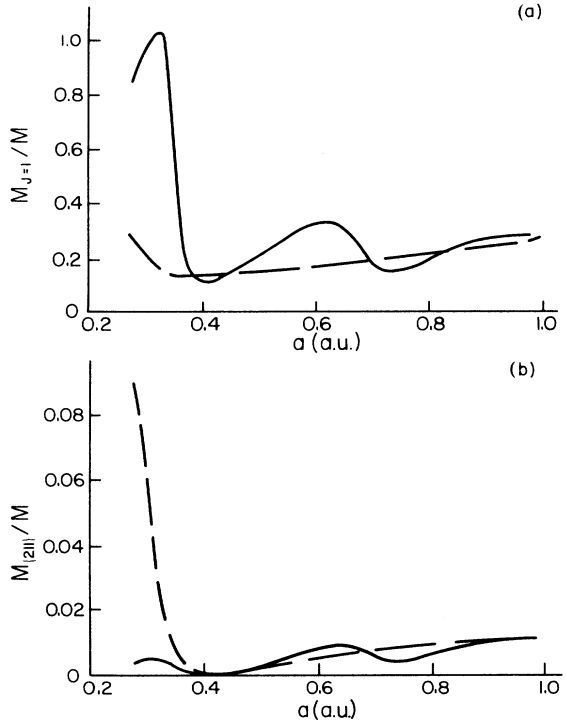

FIG. 6. Fraction of the total matrix element going into a single channel. The conditions are identical to those in Fig. 3, except we look at the ionization of a $2s$ electron. The dipole contribution is allowed to be larger than the total matrix element because the cross terms ($j\neq j'$) can be negative. Note the difference in scale between Figs. 3(b) and 6(b).

V. CONCLUSIONS

We have presented strong evidence of the presence of two approximate selection rules in the ionization of a

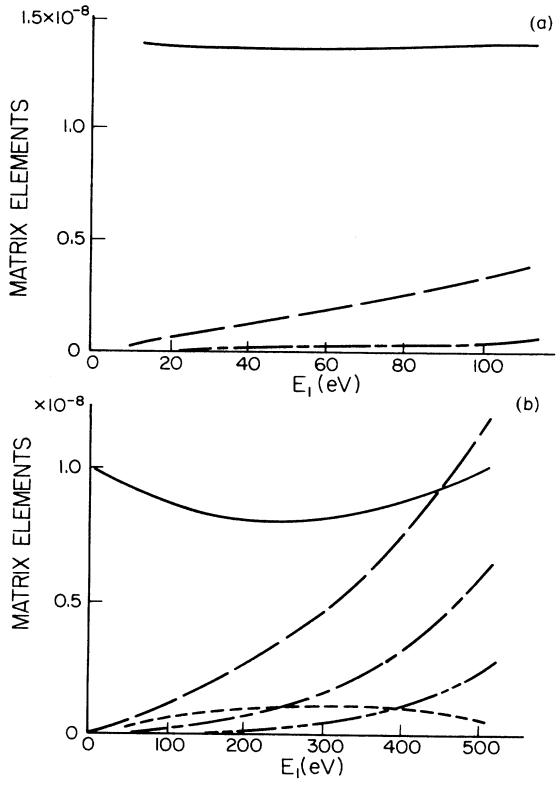

FIG. 7. Matrix elements for the $1s$ ionization of an electron in a Coulomb potential with $Z=10.66$, approximating the continuum wave functions by plane waves. (a) $E_i=100$ eV above threshold. (——) {000} channel, (— —) {110} channel, and (—·—) {220} channel. (b) $E_1=500$ eV above threshold. The notation is the same as in (a). (— — —) is the {211} channel and (—··—) is the {330} channel.

core level by an incident electron, over the energy range of relevance to absorption structure experiments. The first approximate selection rule states that the dipole part of the Coulomb interaction between the two electrons dominates the interaction at all energies above threshold. The second approximate rule says that the dominant channel of the interaction is one in which the two final-state electrons both have angular momentum l_c+1, where l_c is the angular momentum of the core electron. It also predicts that the l_c+2 component of the incident electron wave function drives the interaction. The calculations done to support these approximate rules include both realistic atomic single-particle potentials and parametrized model potentials, which can be easily changed to elucidate behavior. We have shown that these rules are valid only when the core potential supports an l_c+1 resonance or discrete level in addition to the initial bound state with l_c. Also, we find empirically that the core electron's wave function must be nodeless; e.g., the rules hold for K- and $L_{2,3}$-edge processes, but not for L_1 or $M_{2,3}$ ionizations. The trends become stronger for a given l_c as the binding energy of the core state increases.

The approximate selection rules found above are of particular interest in studying electron-induced extended fine-structure experiments such as EAPFS.[45] We have shown that one must be cautious in applying EAPFS to light elements, where the core state is not sufficiently deeply bound. When the approximate rules apply, both of the final-state electrons tend to have the same angular momentum as an EXAFS final-state electron would have, l_c+1. Thus the incident electron energy derivative of the oscillatory part of the EAPFS ionization rate should contain the same information as an EXAFS absorption coefficient, as outlined in the Introduction. In a subsequent paper[13] we will examine this claim more fully. We shall also show that the approximate selection rules hold in model systems which closely approximate the core environment of a real metallic system.

ACKNOWLEDGMENTS

This work was supported by Department of Energy Contract No. DE-AS05-79ER10427 and Grant No. DE-FG05-84ER45071. Computer facilities were supplied by the Computer Science Center of the University of Maryland. G. W. Bryant provided the computer code for integrating Schrödinger's equation. We would also like to thank G. W. Bryant, G. E. Laramore, and J. F. Morar for useful discussions. H. Griem and V. L. Jacobs offered helpful comments on the manuscript. One of us (T.L.E.) benefited from helpful conversations with J. J. Rehr, R. L. Martin, G. Wendin, and S. M. Younger.

APPENDIX: THE OPW APPROXIMATION

Since our primary objective in this project was to determine the ordering of the channels and whether one predominated, rather than to produce precise values of the matrix elements, it was hoped that a simpler calcula-

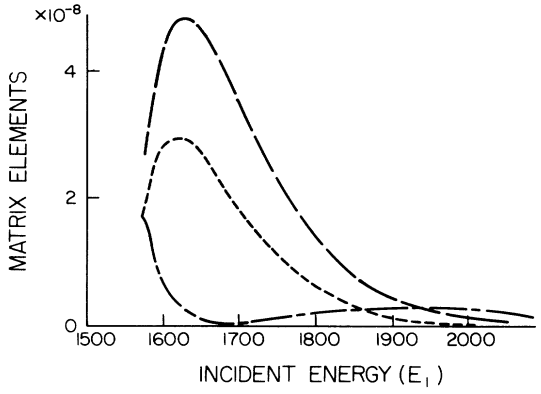

FIG. 8. Matrix elements for the ionization of a 1s electron from a Coulomb potential with $Z=10.66$, in the OPW approximation when the continuum wave functions are orthogonalized to the 1s, 2s, and 2p core levels. One of the final-state electrons is fixed at $E_2=E_F=11.7$ eV. (——) is the {110} channel, (— — —) the {211}, and (—·—) the {101}.

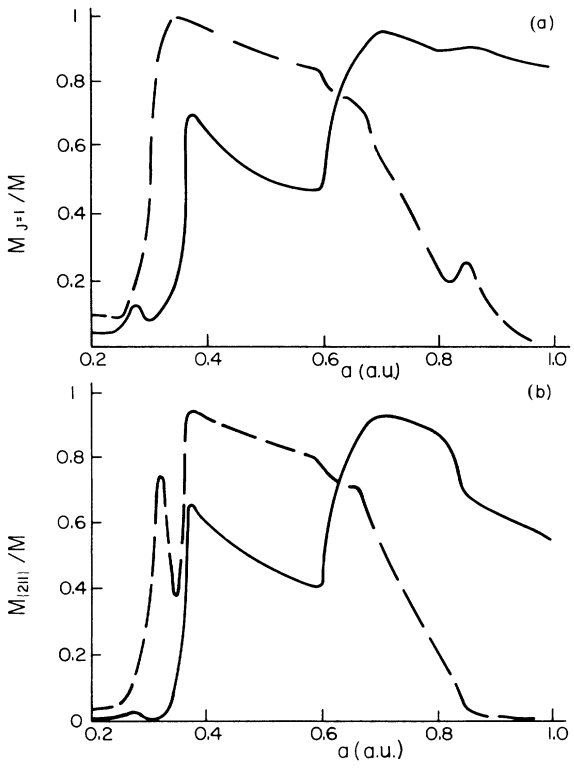

FIG. 9. Fraction of the total matrix element going into a single channel in the OPW approximation. Shown is the K-edge excitation of the Yukawa potential with $Z=13$. The continuum wave functions are orthogonalized to the bound states of the potential. The notation is the same as in Fig. 3.

tion would have sufficed. As alluded to earlier, such was not the case. Williams and Shirley[46] offered a caution. Since those calculations did not need to look at the angular momentum dependence of the matrix elements, they were not a clear guide. We conjectured that OPW calculations would generally provide qualitative trends in ordering for energies at least away from presumably spurious dips. The previous advertisement[5,6] of a monopole selection rule was based on a crude calculation involving (1) no angular momentum combinatorics, and (2) orthogonalization to the core state of only the final-state plane wave into which the core electron hopped, but (3) a rather good treatment of the core wave function.[47]

Using a hydrogenlike wave function for the core electron, and plane waves for the continuum electrons:

$$\phi_{kl}^{\mathrm{PW}}(r)=\left[\frac{2}{\pi}\right]^{1/2} krj_l(kr) , \tag{A1}$$

where $j_l(x)$ is the regular spherical Bessel function of order l. We calculate the K-edge matrix elements (4) and plot them in Fig. 8. The core states used are the bound states of the Coulomb potential with charge $Z=10.66$, chosen so that binding energy of the $1s$ electron is comparable to that of the aluminum $1s$ level. Here the $\{000\}$ level is the largest, with the $\{211\}$ (the largest channel in the exact case) barely visible on the graph. This type of calculation led to the earliest thought that a monopole selection rule might dominate in EAPFS.[48]

We next try an orthogonalized plane wave (OPW) approximation, still keeping the hydrogenic core state. OPW is still popular for this type of problem.[49] The radial wave functions (A1) are replaced by

$$\phi_{kl}^{\mathrm{OPW}}(r)=\phi_{kl}^{\mathrm{PW}}(r)-\sum_n (u_{nl},\phi_{kl}^{\mathrm{PW}})u_{nl}(r) , \tag{A2}$$

where u_{nl} is the radial component of one of the bound-state wave functions, and (a,b) is the scalar product for radial wave functions. The sum is over all bound states of angular momentum l. In Fig. 9 we show typical matrix elements for the $Z=10.66$ hydrogenlike potential, where one of the outgoing electrons (l_2) is fixed at the Fermi level. This should approximate the rigorous matrix element calculation. The $\{211\}$ matrix element falls off much more rapidly than in our model calculations; here the $\{110\}$ channel dominates. Thus the standard OPW calculation is not useful for reliable EAPFS calculations.

If we use our Yukawa potential (7) to generate the core states, we find for $Z=13$ the results in Fig. 9. Comparing with Fig. 3, we see that the OPW approximation errs dramatically in calculating the total matrix element. In addition, OPW does rather poorly in predicting the approximate selection rules. These figures, however, give some insight into the flaws of the OPW approximation in this problem. The sharp breaks in the OPW matrix element, dipole fraction, and EXAFS-like channel fraction as a function of the screening length a appear to be correlated with the onset of a new bound state. For example, the sharp rise in the OPW matrix element at $a\approx 0.4$ coincides with the appearance of the $2p$ bound state of the $Z=13$ Yukawa potential.[50]

---

*Current address: Naval Research Laboratory, Code 4684, Washington, D.C. 20375.

[1]H. Froitzheim, in *Electron Spectroscopy for Surface Analysis,* edited by H. Ibach (Springer, Berlin, 1977), p. 205; G. Ertl and J. Küppers, *Low Energy Electrons and Surface Chemistry* (Chemie, Weinheim, 1974), Chap. 3, and references therein.

[2]Gerald D. Mahan, *Many-Particle Physics* (Plenum, New York, 1981), Sec. 8.3 and references therein; A. Temkin, Phys. Rev. Lett. **49**, 365 (1982).

[3]J. H. Moore, J. A. Tossell, and M. A. Coplan, Accounts Chem. Res. **15**, 192 (1982); I. E. McCarthy and E. Weingold, Phys. Rep. **27C**, 275 (1976); A. Giardini-Guidoni, R. Fantoni, R. Camilloni, and G. Stefani, in *Emission and Scattering Techniques,* edited by Peter Day (Reidel, Dordrecht, 1981), p. 293.

[4]S. M. Younger, Phys. Rev. A **22**, 111 (1980).

[5]E.g., M. L. denBoer, T. L. Einstein, W. T. Elam, Robert L. Park, L. D. Roelofs, and G. E. Laramore, Phys. Rev. Lett. **44**, 496 (1980).

[6]For more detailed reviews, see T. L. Einstein, Appl. Surf. Sci. **11/12**, 42 (1982); T. L. Einstein and R. L. Park, in *Extended X-ray Absorption Fine Structure,* edited by R. W. Joyner (Plenum, New York, in press), Chap. 10.

[7]G. E. Laramore, Surf. Sci. **81**, 43 (1979).

[8]P. I. Cohen, T. L. Einstein, W. T. Elam, Y. Fukuda, and R. L. Park, Appl. Surf. Sci. **1**, 538 (1978).

[9]*EXAFS and Near Edge Structure,* edited by A. Bianconi, L. Incoccia, and S. Stipcich (Springer, Berlin, 1979).

[10]A. Kotoni and Y. Toyogawa, in *Synchrotron Radiation: Techniques and Applications,* edited by C. Kunz (Springer, Berlin, 1979), Chap. 4.

[11]For a review of EXAFS, see P. A. Lee, P. H. Citrin, P. Eisenberger, and B. M. Kincaid, Rev. Mod. Phys. **53**, 769 (1981).

[12]S. T. Manson and J. W. Cooper, Phys. Rev. **165**, 126 (1968); S. T. Manson, in *Photoemission in Solids I: General Principles,* edited by M. Cardona and L. Ley (Springer, Berlin, 1978), p. 135.

[13]M. J. Mehl, T. L. Einstein, and G. W. Bryant (unpublished).

[14]M. R. H. Rudge, Rev. Mod. Phys. **40**, 564 (1968); F. W. Byron, Jr. and C. J. Joachain, Phys. Rev. A **8**, 1267 (1973).

[15]S. Geltman, J. Phys. B **7**, 1994 (1974), studies the double ionization of helium; his Coulomb-projected Born approximation (with or without exchange) adequately replicates experiments.

[16]M. R. H. Rudge and S. B. Schwartz, Proc. Phys. Soc. London **88**, 579 (1966); **88**, 563 (1966).

[17]M. Blaha and J. Davis, Naval Research Laboratory Memorandum Report No. 4245, 1980 (unpublished).

[18]J. J. Rehr, E. A. Stern, R. L. Martin, and E. R. Davidson, Phys. Rev. B **17**, 560 (1978); P. A. Lee and G. Beni, *ibid.* **15**, 2862 (1977).

[19]E. A. Stern and J. J. Rehr, Phys. Rev. B **27**, 3351 (1983); U. von Barth and G. Grossman, *ibid.* **25**, 5150 (1982).

[20]G. W. Bryant, J. Phys. F **10**, 321 (1980) and references therein. However, see Ref. 24 for another point of view.

[21]W. H. E. Schwarz, Angew. Chem. Int. Ed. Engl. **13**, 454 (1974); D. A. Shirley, Chem. Phys. Lett. **16**, 220 (1972); A. R. Williams and N. D. Lang, Phys. Rev. Lett. **40**, 954 (1978).

[22]L. C. Davis and L. A. Feldkamp, Phys. Rev. B **23**, 4269 (1981).

[23]E.g., W. L. Schaich, Phys. Rev. B **29**, 6513 (1984).

[24]J. P. Perdew and A. Zunger, Phys. Rev. B **23**, 5048 (1981); O. Gunnarsson and B. I. Lundqvist, *ibid.* **13**, 4274 (1976).

[25]A. Zangwill, in *EXAFS and Near Edge Structure III,* edited by K. O. Hodgson, B. Hedman, and J. E. Penner-Hahn (Springer, Berlin, 1984). See also A. Zangwill and D. A. Liberman, J. Phys. B **17**, L253 (1984).

[26]The idea that the slower electron, the one at E_F, is affected by higher charge is reminiscent of approximations (A6) and (A7) of Ref. 17; however, we did not allow for k-dependent effects. The majority of our calculations then are in some sense similar to their approximation (A8), using the bare atomic charge for both electrons. A screened charge is also used in Ref. 16.

[27]M. S. Woolfson, S. J Gurman, and B. W. Holland, Surf. Sci. **117**, 450 (1982).

[28]Shih Hung Chou, Ph.D. thesis, University of Washington, 1982 (unpublished).

[29]S. M. Younger, in *Electron Impact Ionization,* edited by T. D. Maerk and G. H. Dunn (Springer, Vienna, 1985), Chap. 1.

[30]Cf., e.g., S. Flügge, *Practical Quantum Mechanics* (Springer, Berlin, 1974).

[31]D. M. Brink and G. R. Satchler, *Angular Momentum,* 2nd ed. (Clarendon, Oxford, 1968).

[32]B. K. Teo and P. A. Lee, J. Am. Chem. Soc. **101**, 2815 (1979).

[33]For experimental evidence, see S. M. Heald and E. A. Stern, Phys. Rev. B **16**, 5549 (1977); D. Denley, R. S. Williams, P. Perfetti, D. A. Shirley, and J. Stöhr, *ibid.* **19**, 1762 (1979).

[34]P. Hohenberg and W. Kohn, Phys. Rev. **136**, B864 (1964).

[35]F. Herman and S. Skillman, *Atomic Structure Calculations* (Prentice-Hall, New York, 1963).

[36]W. E. Pickett and C. S. Wang, Phys. Rev. Lett. **51**, 597 (1983); J. P. Perdew and M. Levy, *ibid.* **51**, 1884 (1983); L. J. Sham and M. Schlüter, *ibid.* **51**, 1888 (1983).

[37]E.g., L. Reimer, *Transmission Electron Microscopy* (Springer, Berlin, 1983).

[38]T. L. Einstein, L. D. Roelofs, Robert L. Park, and G. E. Laramore, Bull. Am. Phys. Soc. **24**, 506 (1979).

[39]E.g., G. W. Bryant, Ph.D. thesis, Indiana University, Bloomington, Indiana, 1979 (unpublished).

[40]G. Wendin (private communication).

[41]K. Siegbahn *et al., ESCA. Atomic, Molecular and Solid State Structures Studied by Means of Electron Spectroscopy* (Almqvist and Wiksells, Uppsala, 1967).

[42]J. F. Morar and R. L. Park, J. Vac. Sci. Technol. A **1**, 1043 (1983).

[43]M. DeCrescenzi *et al.*, in *EXAFS and Near Edge Structure,* Ref. 9, pp. 382, 394, and 397; M. DeCrescenzi, F. Antonangeli, C. Bellini, and R. Rosei, Solid State Commun. **46**, 875 (1983); Phys. Rev. Lett. **50**, 1949 (1983); M. DeCrescenzi, L. Papagno, G. Chiarello, R. Scarmozzino, E. Colavita, R. Rosei, and S. Mobilio, Solid State Commun. **40**, 613 (1981). L. Papagno, M. DeCrescenzi, G. Chiarello, E. Colavita, R. Scarmozzino, L. S. Caputi, and R. Rosei, Surf. Sci. **117**, 525 (1982).

[44]T. Tyliszczak and A. P. Hitchcock, J. Vac. Sci. Technol. A **4**, 1372 (1986). See also D. K. Saldin, in *The Structure of Surfaces-II,* edited by J. F. van der Veen and M. A. Van Hove (Springer, Berlin, in press).

[45]T. L. Einstein, M. J. Mehl, J. F. Morar, R. L. Park, and G. E. Laramore, Appl. Surf. Sci. **1**, 391 (1978).

[46]R. S. Williams and D. A. Shirley, J. Chem. Phys. **66**, 2378 (1977), showed that OPW correctly predicts the total photoemission cross sections, but is not reliable for the differential cross section, which is essentially what we are measuring here.

[47]D. A. Liberman, J. T. Waber, and D. T. Cramer, Phys. Rev. **137**, A27 (1965). We do not include relativistic corrections (cf. Ref. 4).

[48]G. E. Laramore, Phys. Rev. B **18**, 5254 (1978); and private communication.

[49]E.g., A. J. Glick and A. L. Hagen, Phys. Rev. B **15**, 1950 (1977); Joseph Callaway, *Quantum Theory of the Solid State* (Academic, New York, 1974), Sec. 4.3

[50]Since the sharp structure in the OPW approximation is due to the appearance of bound states, we might remove this effect by orthogonalizing to resonant states as well as bound states. This might improve the overall accuracy of the OPW, but we have no calculations to verify this idea.